Pure Appl. Geophys.
© 2012 Springer Basel (outside the USA)
DOI 10.1007/s00024-012-0491-7

Pure and Applied Geophysics

Near-Field Tsunami Edge Waves and Complex Earthquake Rupture

Eric L. Geist[1]

Abstract—The effect of distributed coseismic slip on progressive, near-field edge waves is examined for continental shelf tsunamis. Detailed observations of edge waves are difficult to separate from the other tsunami phases that are observed on tide gauge records. In this study, analytic methods are used to compute tsunami edge waves distributed over a finite number of modes and for uniformly sloping bathymetry. Coseismic displacements from static elastic theory are introduced as initial conditions in calculating the evolution of progressive edge-waves. Both simple crack representations (constant stress drop) and stochastic slip models (heterogeneous stress drop) are tested on a fault with geometry similar to that of the $M_w = 8.8$ 2010 Chile earthquake. Crack-like ruptures that are beneath or that span the shoreline result in similar longshore patterns of maximum edge-wave amplitude. Ruptures located farther offshore result in reduced edge-wave excitation, consistent with previous studies. Introduction of stress-drop heterogeneity by way of stochastic slip models results in significantly more variability in longshore edge-wave patterns compared to crack-like ruptures for the same offshore source position. In some cases, regions of high slip that are spatially distinct will yield sub-events, in terms of tsunami generation. Constructive interference of both non-trapped and trapped waves can yield significantly larger tsunamis than those that produced by simple earthquake characterizations.

1. Introduction

Tsunamis generated along a continental shelf exhibit interesting behavior, particularly with regard to the excitation of edge waves (Carrier, 1995). Edge waves are waves fixed by refraction, propagating parallel to the shoreline. Continental subduction zone earthquakes typically result in coseismic vertical displacement over the shelf and on land, as opposed to displacement in deep water associated with, for example, slow tsunami earthquakes. Notable examples of shelf tsunamis of this type are the 1952 Kamchatka tsunami (MacInnes *et al.*, 2010) and the 2010 Chile tsunami (Fritz *et al.*, 2011). The $M_w = 9.0$ 1952 Kamchatka subduction zone earthquake (Bürgmann *et al.*, 2005; Johnson and Satake, 1999), was efficient at generating tsunami edge waves. The arrival of maximum tsunami amplitudes observed in Japan for this event are consistent with the group velocity of the fundamental edge-wave mode and development of an edge-wave Airy phase (Abe and Ishii, 1987; Golovachev *et al.*, 1992). The $M_w = 8.8$ 2010 Chile tsunami also generated significant edge wave activity. The complex rupture associated with this and other subduction zone earthquakes often result in sub-events with spatially distinct regions of coseismic displacement (Kiser and Ishii, 2011; Lay *et al.*, 2010; Pollitz *et al.*, 2011). Each sub-event can produce its own set of edge waves. The progressive edge waves eventually resonate, owing to the geometry of the coastline and shelf, resulting in prolonged duration of tsunami wave activity (Yamazaki and Cheung, 2011). Field evidence of different flow directions for the tsunami (Morton *et al.*, 2011) may also be explained by oppositely propagating edge waves.

Near-field tsunami edge waves are often distinguished from broadside waves (Carrier, 1995). Broadside waves are local waves propagating directly from the source in a direction approximately perpendicular to strike. The largest local runup is often associated with broadside waves, although for landslide tsunamis, Lynett and Liu (2005) note that the maximum edge wave amplitude can exceed the maximum broadside amplitude. Because of the short propagation distance of non-trapped waves, it can be established that variations in slip patterns for a given seismic moment and fault dimensions directly affect the runup distribution (Geist, 2002; McCloskey *et al.*, 2007; McCloskey *et al.*, 2008). In these

[1] U.S. Geological Survey, 345 Middlefield Rd., MS 999, Menlo Park, CA 94025, USA. E-mail: egeist@usgs.gov

Published online: 22 May 2012

studies, a stochastic slip model was used to vary slip according to a power-law spectrum in the radial wavenumber domain along the fault plane. Moreover, the power-law exponent for slip can be related to the power-law exponent of the far-field seismic displacement spectrum (Andrews, 1980; Herrero and Bernard, 1994; Tsai, 1997).

Geist (2009) hypothesized that in general, details of the slip distribution pattern affect the behavior of edge waves. Because the initial tsunami wavefield provides the initial conditions for edge wave propagation, it is logical to assume that slip variations affect edge waves through the calculation of vertical displacement of the sea floor and the initial tsunami wavefield. As will be shown, however, edge wave properties depend on both the strike-parallel spectrum of the initial wavefield and offshore distance; thus it is difficult to make a direct connection between slip patterns and edge waves as it is for broadside waves.

In this paper, the relationship between realistic earthquake rupture and edge wave characteristics is examined. In Sect. 2, the development of edge wave theory, particularly as it relates to tsunami initial conditions, is reviewed. In place of analytic functions of sea floor displacement that have been used for edge wave initial conditions in the past, sea floor displacement is calculated from simple crack models (Sect. 3) and stochastic slip models (Sect. 4). The timing and spatial distribution of maximum tsunami amplitude at the coast is examined to determine how it varies with different representations of the earthquake source. Results enhance understanding of the near-field hazard associated with continental shelf tsunamis.

2. Method

The evolution of edge waves can be derived exactly for uniformly sloping bathymetry of the continental shelf ($z = -h(x) = -x\tan\beta = -xs$ see Fig. 1). Consider the linear long-wave equations

$$\frac{\partial\zeta}{\partial t} + \nabla\cdot(h\mathrm{u}) = 0 \quad \text{and} \quad \frac{\partial \mathrm{u}}{\partial t} + \mathrm{g}\nabla\zeta = 0, \qquad (1)$$

where ζ is the sea surface elevation and $\mathbf{u}$ is the horizontal velocity field. Inclusion of the non-linear terms of the shallow-water wave equations in the development of edge-wave theory is discussed by Carrier (1995). Substituting for $\mathbf{u}$ results in the hyperbolic partial differential equation

$$\frac{\partial^2\zeta}{\partial t^2} - g\nabla\cdot(h\nabla\zeta) = 0. \qquad (2)$$

The wave field is then separated between a cross-shore wave function (η) and periodic solutions in the longshore direction (y) and in time (t):

$$\zeta(x, y, t) = \eta(x)e^{i(k_y y - \omega t)}. \qquad (3)$$

Substituting into Eq. 2 results in the second-order ordinary differential equation with respect to η

$$x\frac{\mathrm{d}^2\eta}{\mathrm{d}x^2} + \frac{\mathrm{d}\eta}{\mathrm{d}x} + \left(\frac{\omega^2}{sg} - k_y^2 x\right)\eta = 0. \qquad (4)$$

Using the transformation (Mei *et al.*, 2005)

$$\xi = 2k_y x, \quad \eta = e^{-\xi/2}f(\xi), \qquad (5)$$

the confluent hypergeometric equation is obtained:

$$\xi\frac{\mathrm{d}^2 f}{\mathrm{d}\xi^2} + (1-\xi)\frac{\mathrm{d}f}{\mathrm{d}\xi} + \frac{1}{2}\left(\frac{\omega^2}{k_y sg} - 1\right)f = 0. \qquad (6)$$

This equation is a special case of Kummer's equation, where the general coefficient of the second term in Eq. 6 is given by (b–ξ), and has well known solutions (Dingemans, 1997; Mei *et al.*, 2005):

$$f_1 = M(\gamma, b, \xi) = \sum_{n=0}^{\infty}\frac{(\gamma)_n}{(b)_n}\frac{\xi^n}{n!} \quad \textit{and} \qquad f_2 = U(\gamma, b, \xi), \quad b \neq 0, -1, -2, \ldots, \qquad (7)$$

where

$$\gamma = \frac{1}{2} - \frac{\omega^2}{2k_y sg} \qquad (8)$$

and Pochhammer's notation is used

$$(a)_n = \frac{\Gamma(a+n)}{\Gamma(a)} = a(a+1)(a+2)\ldots(a+n-1), \quad (a)_0 = 1. \qquad (9)$$

The confluent hypergeometric function of the second kind $U(\gamma, 1, \xi)$ is not finite at the shoreline ($\xi \to 0$) (Dingemans, 1997). In addition, $M(\gamma, 1, \xi)$ is

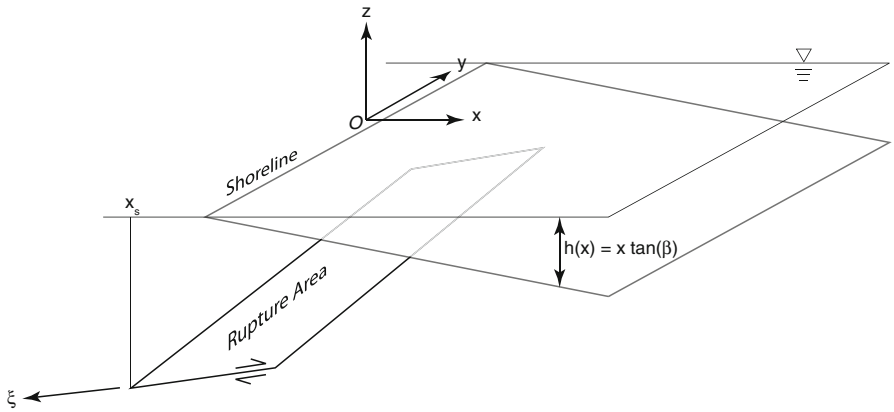

Figure 1
Geometry of uniform sloping bathymetry and rupture along inter-plate thrust fault. ξ-coordinate in line with dip direction of fault. Rupture area straddles the shoreline in this example

finite for $(\xi \to \infty)$ only when $\gamma = 0, -1, -2, \ldots$, which yields the shallow-water, edge-wave dispersion relation.

$$\omega_n^2 = gk_y(2n+1)\tan\beta, \quad n = 0, 1, 2, \ldots. \tag{10}$$

Noting that $M(-n, 1, \xi) = L_n(\xi)$, where $L_n(\xi)$ is the Laguerre polynomial of order n, the cross-shore wave-function can be written as

$$\eta(x) = e^{-k_y x} L_n(2k_y x). \tag{11}$$

The dispersion relation for the nth mode without the long-wave approximation was derived by Ursell (1952):

$$\omega_n^2 = gk_y \sin(2n+1)\beta, \quad n = 0, 1, 2, \ldots, \tag{12}$$

for bottom slope β, provided that $(2n+1)\beta \leq \pi/2$. For small slope and mode number, the two dispersion relations (Eqs. 10, 12) are approximately equal (LeBlond and Mysak, 1978). Ishii and Abe (1980) examine the dispersion relation for shelf profiles other than a uniform slope and find minima in the group velocity in certain cases.

Evidence of edge waves from tide gauge data involves tracking the maximum amplitude arrival along longshore propagation paths. Abe and Ishii (1987) indicate that the maximum amplitude arrival associated with the 1983 Japan Sea tsunami at several tide gauge station along the Niigata coastline closely follows the group velocity expected for edge waves. Golovachev *et al.* (1992) indicate that the maximum amplitude is associated with an Airy phase in edge waves that is possible for a step-like shelf geometry and group velocity minimum. Ishii and Abe (1980) also provide evidence of edge wave arrivals recorded on Japanese tide gauge stations for the 1952 Kamchtka tsunami.

The effect of various source parameters on edge wave excitation, in terms of energy density, was initially examined by Kajiura (1972). In that study, it was noted that the proportion of energy trapped as edge waves in comparison to that radiated into deep water for continental shelf tsunamis increases with decreasing offshore distance of the source and longshore (i.e., strike) dimension of the source. Using a step-like bathymetry for the continental shelf, Kajiura (1972) also demonstrates that edge-wave energy increases with an increasing depth difference between the shelf and deep water. Higher edge wave modes are generated for sources with smaller along-strike length and those located near the shelf edge.

Near-field tsunami edge waves have been considered in terms of an initial-value problem in the context of continental-shelf tsunamis by Carrier (1995), who determines the wavefield in transformed coordinates to calculate runup, and by Fujima *et al.* (2000). The wavefield near the tsunami source can be considered in terms of a Fourier-Laguerre polynomial expansion (cf., Eq. 3), with coefficients a_n:

$$\zeta(x,y,t) = \int_{-\infty}^{\infty} \sum_{n=0}^{\infty} a_n(|k_y|) e^{-|k_y|x} L_n(2|k_y|x) e^{-ik_y y} \times \left(e^{-i\omega t} + e^{i\omega t}\right) \mathrm{d}k_y. \quad (13)$$

At $t = 0$, a set of Fourier coefficients c_{ky} can be set equal to the Laguerre polynomial expansion above, such that

$$c_{k_y}(x) = \sum_{n=0}^{\infty} 2a_n(|k_y|) e^{-|k_y|x} L_n(2|k_y|x). \quad (14)$$

Using the orthogonality property of the Laguerre polynomials, it can then be shown (Carrier, 1995; Morse and Feshbach, 1953) that

$$a_n(|k_y|) = |k_y| \int_0^{\infty} c_{k_y}(x) e^{-|k_y|x} L_n(2|k_y|x)\, \mathrm{d}x. \quad (15)$$

Thus, one can determine the longshore Fourier coefficients from any arbitrary initial displacement and then calculate the Fourier-Laguerre coefficients a_{n} from the above equation. From this, the wavefield can be computed at any time t. Fujima *et al.* (2000) provide computational details regarding the above method. Koshimura *et al.* (1999) relates aspects of the foregoing analysis to obliquely incident, far-field tsunamis as well.

Coseismic vertical displacement of the sea floor that provides the initial conditions for tsunami wave propagation is caused by elastic deformation of the solid earth in response to slip on a fault. Whereas analytic functions resembling the dimensions of coseismic displacement were used by Carrier (1995) and Fujima *et al.* (2000) to develop the theory of near-field tsunami edge waves, realistic initial conditions need to be considered from elastic deformation theory and models. There are several fundamental differences between previous analytic initial conditions and earthquake-derived displacement patterns. One is the length scale of the displacement, which is more extensive in the strike-parallel and strike-normal directions for a $M \sim 8$–9 earthquake than considered by Fujima *et al.* (2000). A second fundamental difference is the presence of landward subsidence in addition to the seaward region of uplift, compared to the one-sided (positive) analytic functions used by Kajiura (1972), Carrier (1995), and Fujima *et al.* (2000). The effect of a dipole displacement pattern on edge wave excitation from simple crack representations of the earthquake is the subject of Sect. 3. In Sect. 4, the effect of heterogeneous slip on edge waves is examined.

Because the phase speed of edge waves is orders of magnitude lower than the rupture velocity of earthquakes, static displacement models are examined to simplify the analysis and reduce the number of independent variables. In addition, because the coseismic vertical displacement occurs primarily on the low bathymetric gradient continental shelf in this study, the effect of horizontal displacements as explained by Tanioka and Satake (1996) will not be examined.

3. *Results: Crack Model*

Because the earthquake ruptures of interest for continental shelf tsunamis are at significant depth (20–50 km in the case of the 2010 Chile earthquake) and do not reach the surface, simple crack models can be used to specify the initial conditions for edge wave propagation. In these cases, the static stress drop associated with the earthquake ($\Delta\sigma$) is approximately uniform (Rudnicki and Wu, 1995). A more complete analysis of the stress drop associated with the 2010 Chile earthquake is given by Luttrell *et al.* (2011). In the next section, cases associated with heterogeneous stress drop are examined.

Pure thrust slip (D) on the fault for a tunnel crack of width $2a$ that extends indefinitely in the y direction (Fig. 1) is given by (Dmowska and Rice, 1986; Rice, 1980)

$$D(\xi) = 2(1-\nu)\Delta\sigma\sqrt{a^2 - \xi^2}/\mu, \quad (16)$$

where ν is the Poisson's ratio and μ is the shear modulus for the solid. For an elliptical crack with uniform stress drop over the region $\xi^2/a^2 + y^2/c^2 \leq 1$, slip is given by

$$D(\xi) = A_{ij}\Delta\sigma\sqrt{1 - \xi^2/a^2 - y^2/c}/\mu, \quad (17)$$

where A_{ij} is a matrix of coefficients described in Dmowska and Rice (1986). Displacement at the surface can be determined for these cases from analytic functions (e.g., Dmowska and Kostrov, 1973) or by discretizing the slip regions and using the point-source

expressions derived by Okada (1985). The latter is generally valid if the discretization size of the fault plane element is much smaller than depth to that element (Geist and Dmowska, 1999). For consistency with the stochastic slip model presented in the next section, the discretized approach with a 1 km fault element size is used here.

The vertical displacement for all cases is calculated from pure thrust motion, a fault dip of 18° (dip of the focal plane for the 2010 Chile earthquake) and strike parallel to the shoreline. For both crack models, $a = 50$ km and $c = 125$ km (rupture half-length in the case of the tunnel crack). The domain where wave calculations are performed spans an area of 200 km in the cross-shore direction and 6,000 km in the longshore direction.

The characteristic vertical displacement pattern for a crack model is landward subsidence and seaward uplift (Fig. 2a). The hingeline of the displacement pattern marks zero displacement contour separating the regions of subsidence and uplift. As the depth of rupture increases down dip (x_s varies between −30 and 50 km; see Fig. 1), the hingeline moves toward the coast. At the point where the hingeline is approximately coincident with the coast, the tsunami changes from a dipole source to a monopole source. The difference between dipole and monopole waves can have a significant effects. For non-trapped phases, dipole waves are stable during propagation (Tadepalli and Synolakis, 1996), with little residual wave activity as the tsunami propagates away from the source region. Monopole waves generally result in a decaying oscillatory response (Momoi, 1964; Wu, 1981).

Broadside and edge waves from the ellipsoidal crack are illustrated by plotting the maximum amplitude over the duration of the simulation parallel to the coastline (Fig. 3a). Tsunami amplitudes are normalized with respect to the maximum offshore coseismic displacement ($\zeta_{0\text{–max}}$). Maximum broadside runup occurs for a source position where coseismic subsidence is immediately offshore. For source locations tested that were farther offshore ($x = 20$, $x = 50$ km), the tsunami splits essentially in two, reducing the amplitude by half, in addition to a slight amount of attenuation owing to geometric spreading. Tsunami shoaling amplification is also slight according to Green's Law, owing to the low bathymetric slope used in the calculations ($s = 1/100$).

Edge waves from the ellipsoidal crack generate similar longshore fluctuation patterns for each position of the source (Fig. 3a), except for the most offshore sources ($x = 20$, 50 km) where there is relatively little excitation of edge waves. Edge wave amplitude is greatest for the sources closest to shore. This is consistent with previous findings (e.g., Fujima *et al.*, 2000; Kajiura, 1972) that for sources that are near or span the coastline, much of the total tsunami energy is trapped. Rabinovich *et al.* (2008) demonstrates this for the 2006 and 2007 Kuril Islands

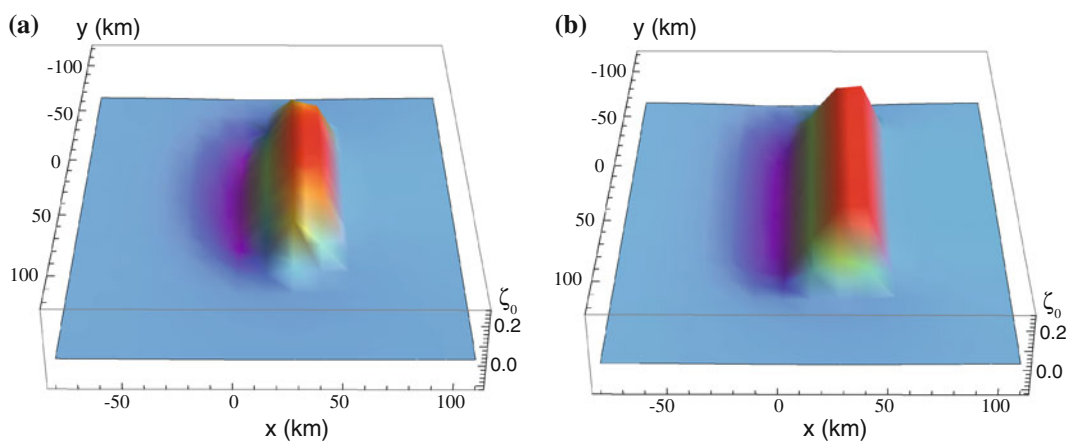

Figure 2
Comparison of vertical displacement pattern (initial tsunami wavefield) for **a** ellipsoidal crack and **b** tunnel crack

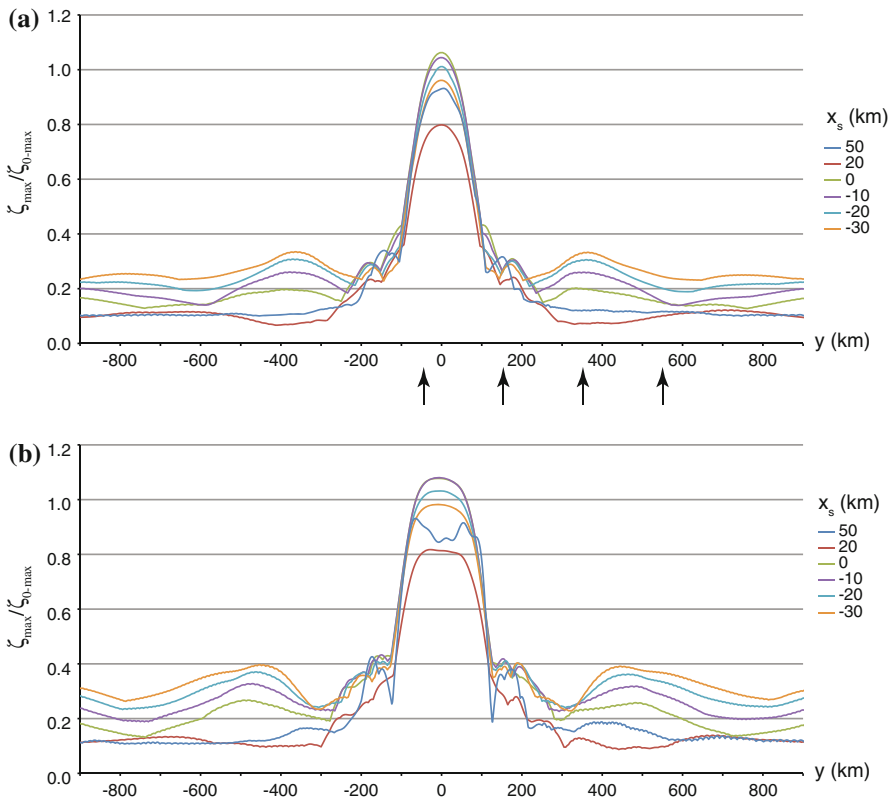

Figure 3
Comparison of maximum amplitude over time, plotted parallel to the coast, for different offshore positions of the source: **a** ellipsoidal crack; **b** tunnel crack. Maximum amplitude normalized with respect to maximum initial amplitude. *Arrows* represent location of time series shown in Fig. 4

tsunamis by comparing the tsunami amplitude distribution derived from observations and modeling. The 2006 event was a subduction zone earthquake that resulted in a significant edge-wave excitation, whereas the 2007 event was an outer-rise earthquake located farther offshore that resulted in little edge-wave excitation.

For nearshore sources in this study, maximum edge wave amplitude occurs approximately 200 km from the end of the rupture zone ($y = \pm 125$ km) and gradually decreases with longshore distance. In comparison to the ellipsoidal crack, the maximum amplitude over time plotted parallel to the coastline for a tunnel crack is shown in Fig. 3b. Although differences in the vertical displacement patterns are subtle (Fig. 2), the tunnel crack appears to be slightly more efficient at generating edge wave energy as evidenced by the overall higher longshore maximum amplitudes (Fig. 3b). The approximate longshore location of the highest edge waves is shifted slightly down shore compared to that for the ellipsoidal crack.

The longshore variations in times series for the nearshore source indicates the dispersive nature of edge waves (Fig. 4a). The first arrival is a non-trapped mode that diminishes in amplitude rapidly away from the source. Conversely, the edge wave packet increasingly develops with distance, in terms of the duration of the packet (cf. Liu *et al.*, 1998). A somewhat regular wave train develops, but not as smooth as for the ideal case examined by Fujima *et al.* (2000). For the offshore source (Fig. 4c), little edge wave energy is generated.

Examination of the Fourier-Laguerre series expansion coefficients (a_n) as a function of longshore wavenumber yields information on which edge wave modes are excited for different source configurations (Fig. 5). Fundamental modes are primarily excited for nearshore sources (Fig. 5a), whereas higher-order

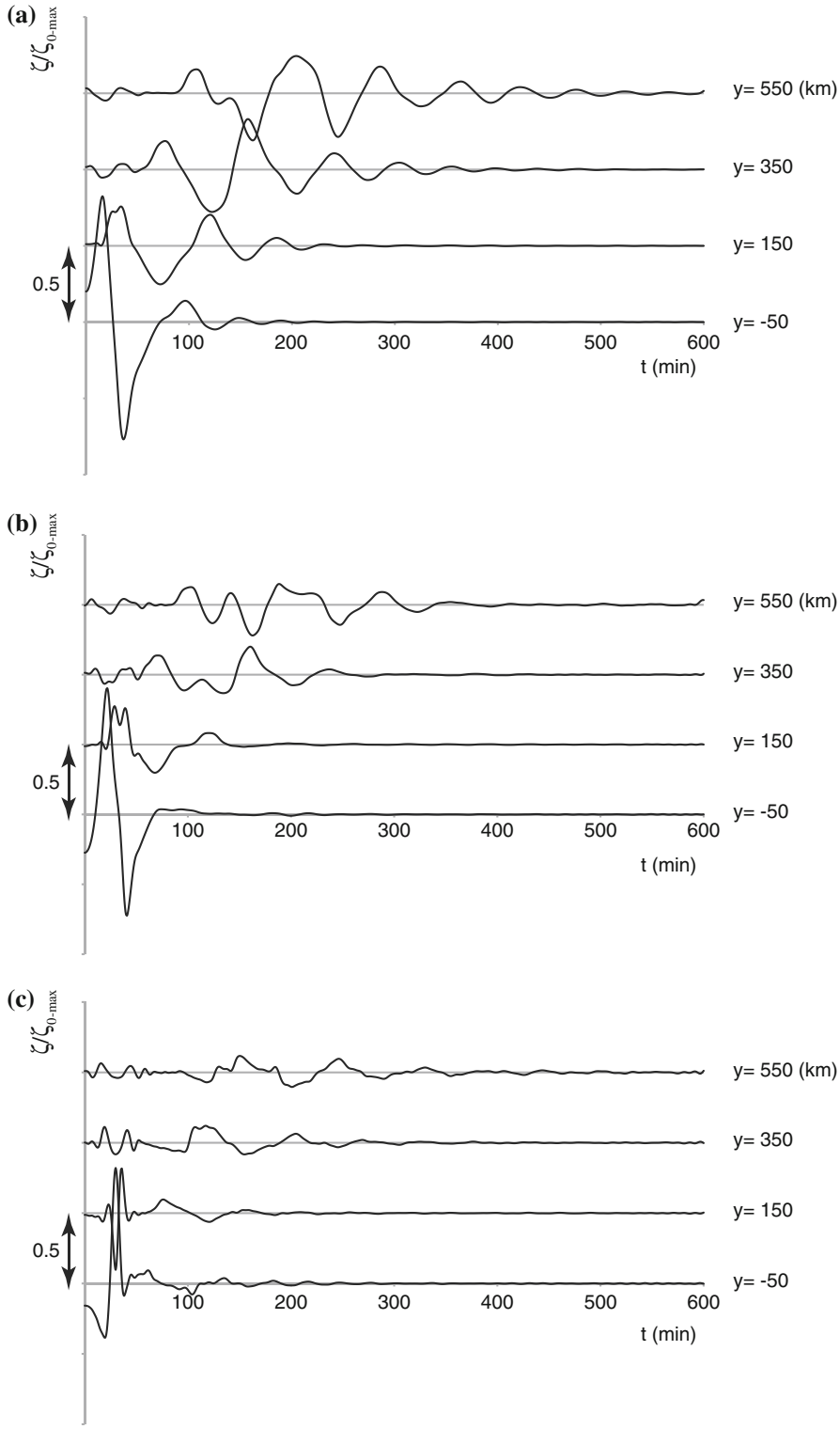

Figure 4
Time series near the coast at different longshore positions using the ellipsoidal crack: **a** $x = -30$ (near shore); **b** $x = 0$; **c** $x = 50$ (offshore)

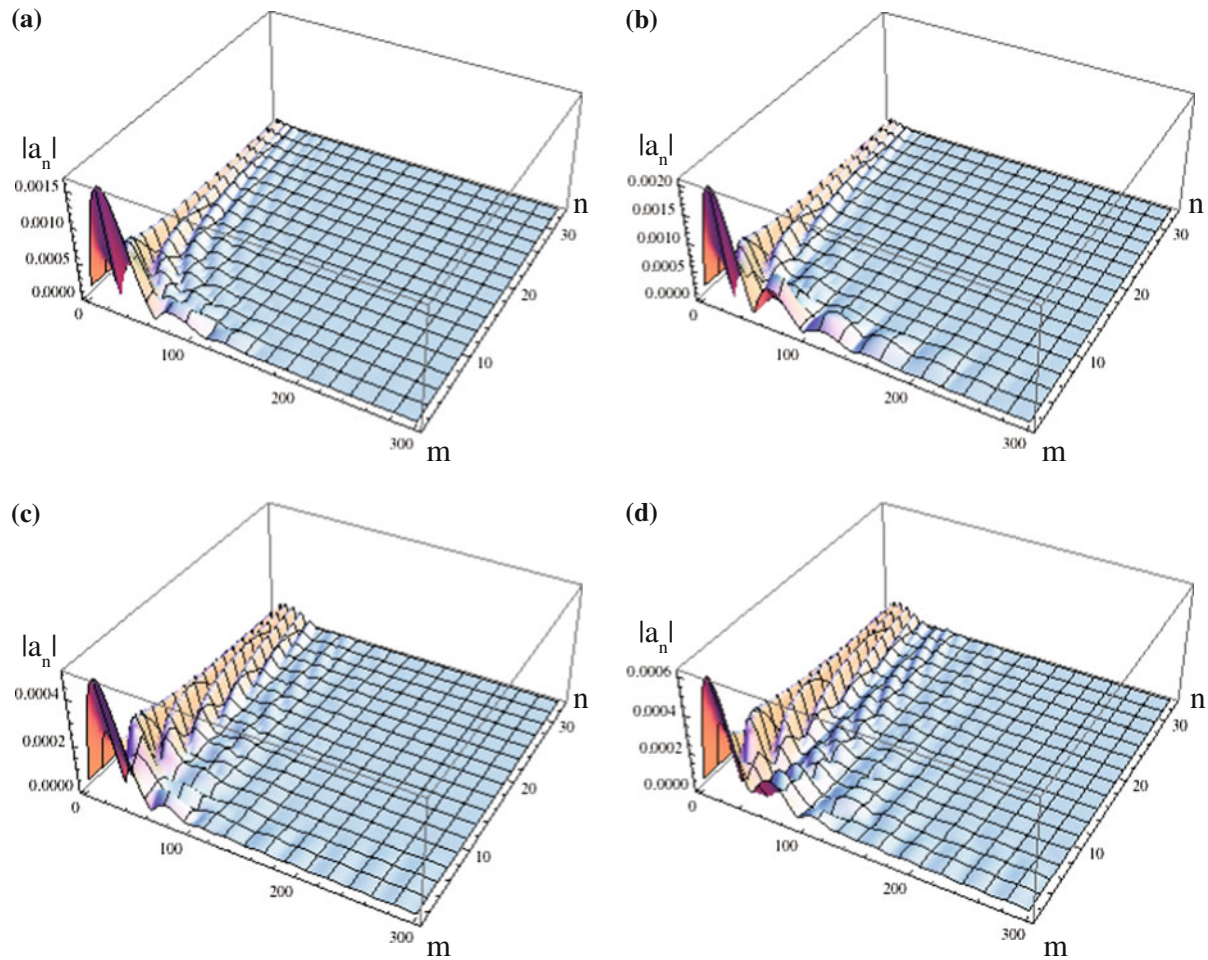

Figure 5
Series expansion coefficients (a_n) as a function of longshore Fourier spectrum (m, where $k_y = 2\pi m/(N_y \Delta_y)$) and edge-wave mode number (n): **a** ellipsoidal crack at nearshore position; **b** tunnel crack at nearshore position; **c** ellipsoidal crack at offshore position; **d** tunnel crack at offshore position

modes become more prominent for offshore sources (Fig. 5c). Comparison of the ellipsoidal and tunnel crack sources (e.g., Fig. 5a, b) shows higher wavenumber components associated with the tunnel crack because of the sharp along-strike slip termination and higher vertical displacement gradients.

4. *Results: Stochastic Slip Model*

Various seismological investigations have established that earthquake rupture is complex and as such, it cannot be characterized by either uniform slip in the case of the dislocation model or uniform stress drop in the case of the crack model. Evidence includes the power-law decay at high wavenumbers of the slip spectrum (e.g., Andrews, 1980; Herrero and Bernard, 1994), inversion of the seismic and geodetic wavefields (Lavallée *et al.*, 2006; Mai and Beroza, 2000, 2002; Tsai, 1997), as well as theoretical arguments (e.g., Koyama, 1994). In this section, we use a recent update to the canonical stochastic slip model (Andrews, 1980) that accounts for large fluctuations of slip (Lavallée *et al.*, 2006) to simulate near-field edge waves. The relationship between stress drop and slip as described by the stochastic source model is discussed by Andrews (1980), Tsai (1997), and Andrews and Barall (2011).

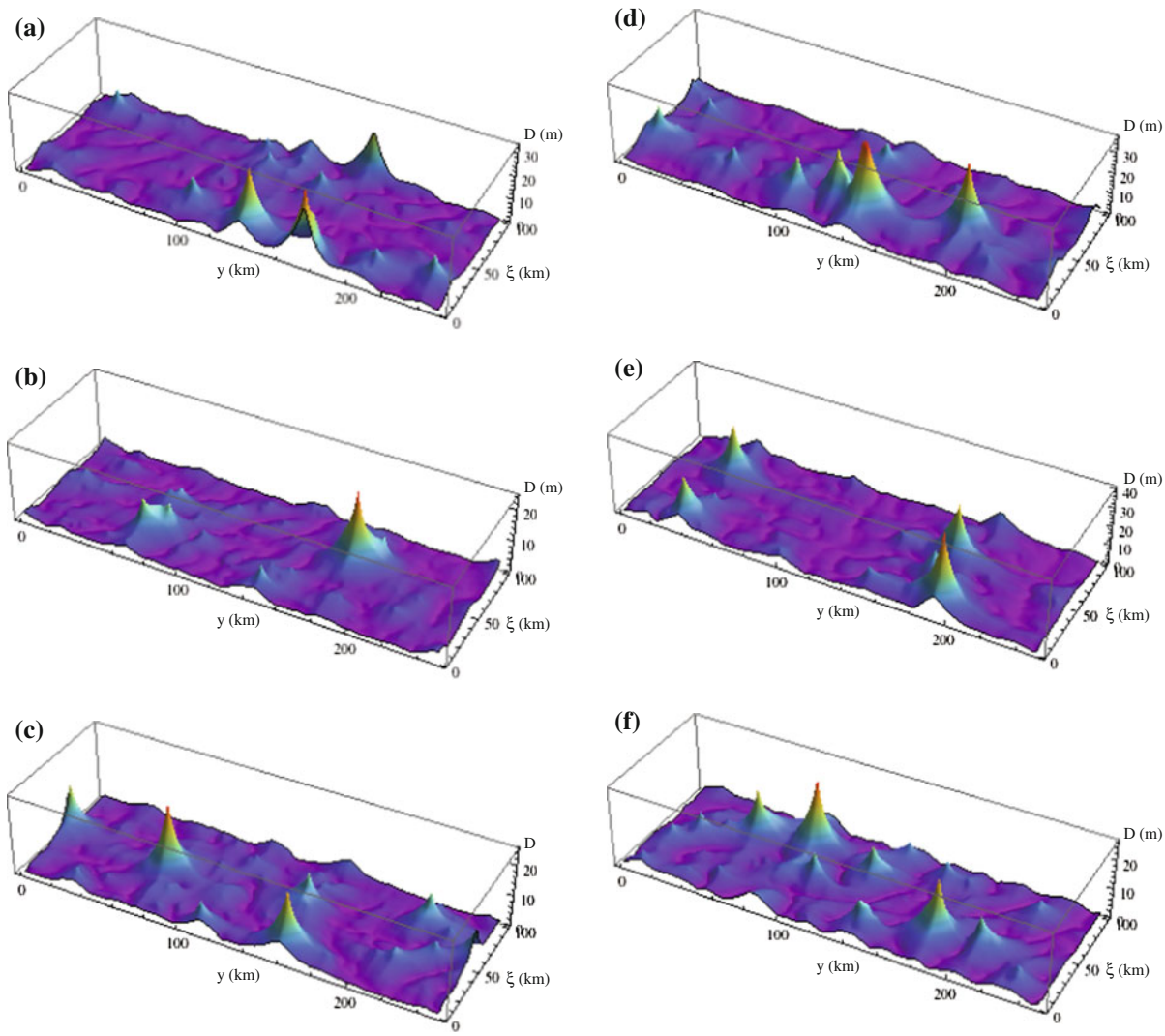

Figure 6
Six slip realizations from the stochastic slip model described in the text. **a** $\bar{D} = 2.59$ m, coefficient of variation (CV) = 1.06; **b** $\bar{D} = 1.74$ m, CV = 1.09; **c** $\bar{D} = 2.24$ m, CV = 0.95; **d** $\bar{D} = 3.48$ m, CV = 1.07; **e** $\bar{D} = 2.92$ m, CV = 1.23; **f** $\bar{D} = 2.72$ m, CV = 0.88

The slip model is specified by a spectrum in the radial wave number domain (k) and two-dimensional random variables that follow a specified probability distribution. The slip spectrum beyond a corner wavenumber (k_c) is given by (Herrero and Bernard, 1994)

$$D(k) = C\frac{\Delta\sigma}{\mu}\frac{L}{k^{\gamma}} \quad k > k_c, \tag{18}$$

where $\Delta\sigma$ is the mean stress drop, μ the shear modulus, L the rupture dimension, and C a constant. The spectral decay exponent γ is linked to the decay of the seismic source spectrum in the frequency domain (Tsai, 1997). Examples of studies where the seismic source spectrum is determined for subduction zone earthquakes include Hartzell and Heaton (1985) and Polet and Kanamori (2000). In the early slip models, the random variables that dictate the self-affine nature of slip (Geist, 2009; Mai and Beroza, 2002) followed a Gaussian distribution (Lavallée *et al.*, 2006). Lavallée and Archuleta (2003) first noted that this slip model does not encompass large variations of slip seen in some seismic inversions.

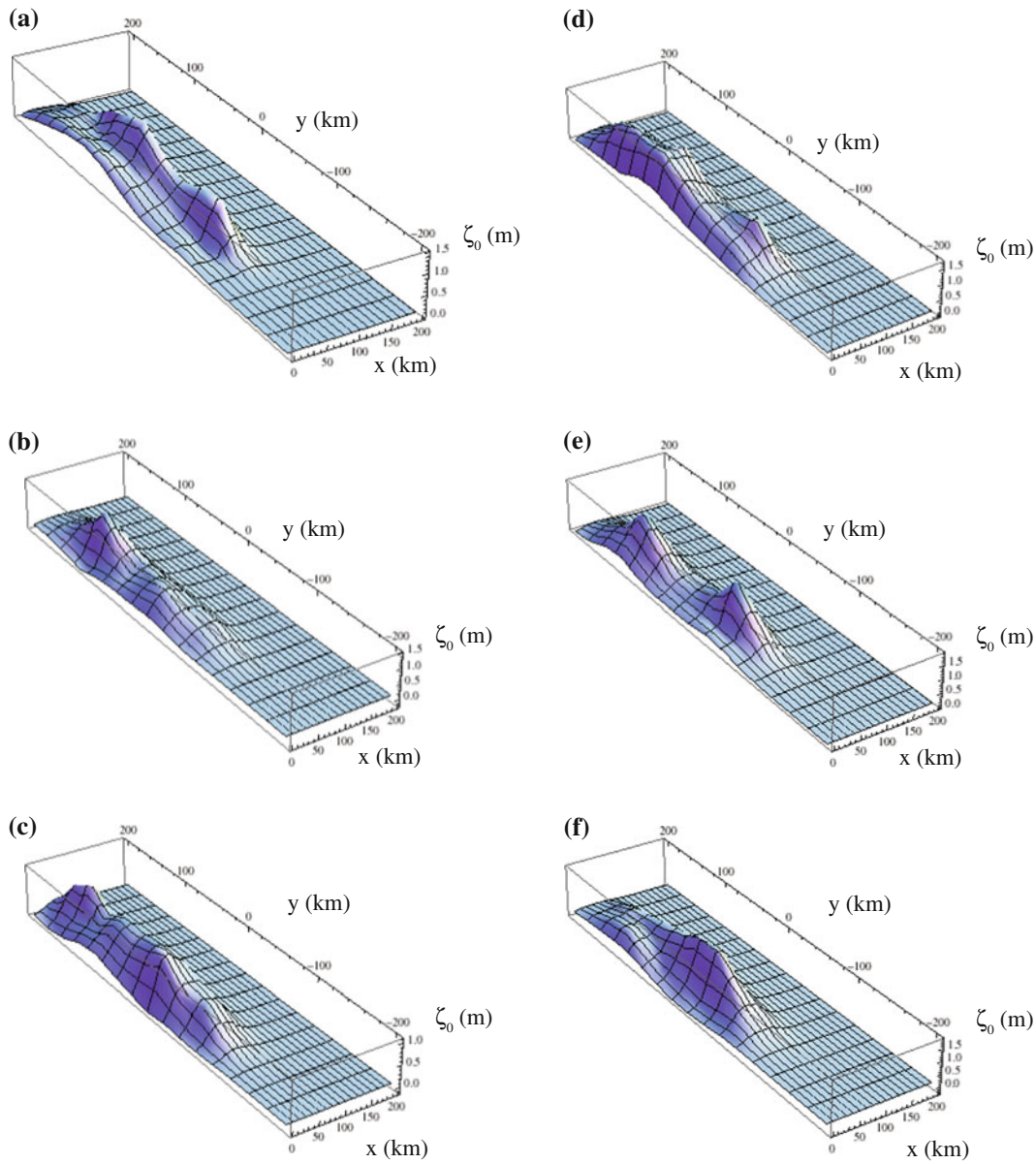

Figure 7
Vertical displacement associated with the six slip realizations shown in Fig. 6. Rupture is located at same offshore position in each case ($x = 0$)

The updated slip model by Lavallée *et al.* (2006) specifies random variables that generally follow a Lévy α-stable distribution (cf., Samorodnitsky and Taqqu, 1994) in which the characteristic function for the distribution is given by:

$$\varphi(k) = \begin{cases} \exp\left\{ik\lambda - c^{\alpha}|k|^{\alpha}\left[1 - i\theta \operatorname{sgn}(k)\tan\frac{\pi\alpha}{2}\right]\right\} & \text{if } \alpha \neq 1 \\ \exp\left\{ik\lambda - c|k|\left[1 - i\theta\frac{2}{\pi}\operatorname{sgn}(k)\ln|k|\right]\right\} & \text{if } \alpha = 1 \end{cases}, \tag{19}$$

where α is a stability parameter $(0<\alpha\leq 2)$, θ a skewness parameter $(-1\leq\theta\leq 1)$, λ a location parameter (real number), and c a scale parameter $(c\geq 0)$. For special cases of the Lévy α-stable distribution, $\varphi(k)$ is the characteristic function for the Gaussian distribution ($\alpha = 2$), Cauchy distribution ($\alpha = 1$ and $\theta = 0$), and Lévy distribution ($\alpha = 1/2$ and $\theta = 1$).

For this study, we use a k^{-2} decay of the slip spectrum and a Cauchy distribution with $\lambda = -1$ and $c = 9.7$, which are reasonable case parameters derived from observations of dip-slip earthquakes (Lavallée *et al.*, 2006; Polet and Kanamori, 2000). Figure 6 shows six slip realizations using these parameters that exhibit different distributions of slip in the dip (ξ) and strike (y) directions. As with the crack models, vertical displacement was calculated using Okada's (1985) point-source expressions and a 1 km grid of fault elements. Figure 7 compares the vertical displacement patterns associated with the slip patterns shown in Fig. 6.

The maximum broadside amplitude, normalized with respect to the maximum initial tsunami amplitude, is often greater than one using the stochastic slip model (Fig. 8), in contrast to the crack models. This is likely caused by constructive interference of non-trapped modes originating from spatially distinct regions of vertical displacement (Geist and Dmowska, 1999), as in the case shown in Fig. 7a. Each of the regions may also act as sub-events and generate their own set of edge waves. Away from the broadside region, the longshore distribution of maximum amplitude from edge waves also varies considerably, depending on the slip distribution. This result confirms the hypothesis suggested in an earlier paper and inferred solely from tsunami measurements that edge wave excitation and amplitude distribution is dependent on slip distribution (Geist, 2009). Correspondingly, there are significant differences in the nearshore time series (Fig. 9) and longshore Fourier spectra (Fig. 10). Although energy is distributed among different edge-wave modes and wavenumbers for each case, the group speed is approximately the same (Fig. 9).\

5. *Discussion*

Results from this study indicate that edge waves are sensitive to the distribution of slip for a continental subduction zone earthquake. It is often difficult to accurately model edge waves using conventional numerical models as described by Liu *et al.* (1998). For this reason, and to extract the dependency of edge wave evolution on initial conditions, the fundamental equations for edge wave propagation along uniformly sloping bathymetry of the continental shelf were implemented using the methods described by Carrier (1995) and Fujima *et al.* (2000). In place of Gaussian-like initial conditions used in these previous studies,

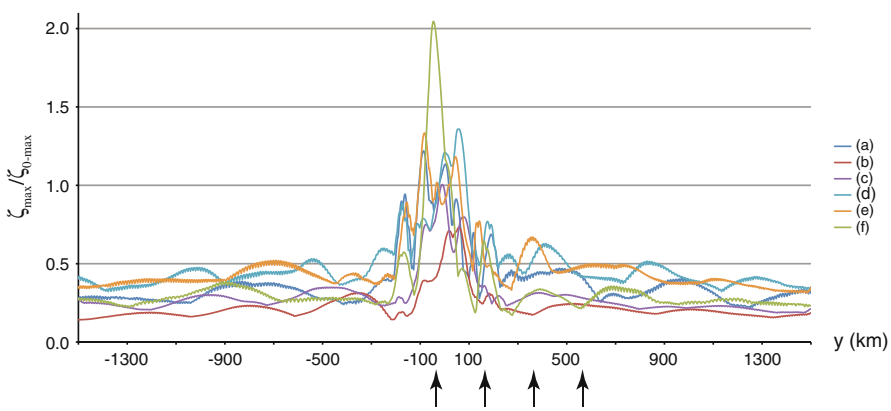

Figure 8
Comparison of maximum amplitude over time, plotted parallel to the coast, for six slip realizations shown in Fig. 6. *Arrows* represent location of time series shown in Fig. 9

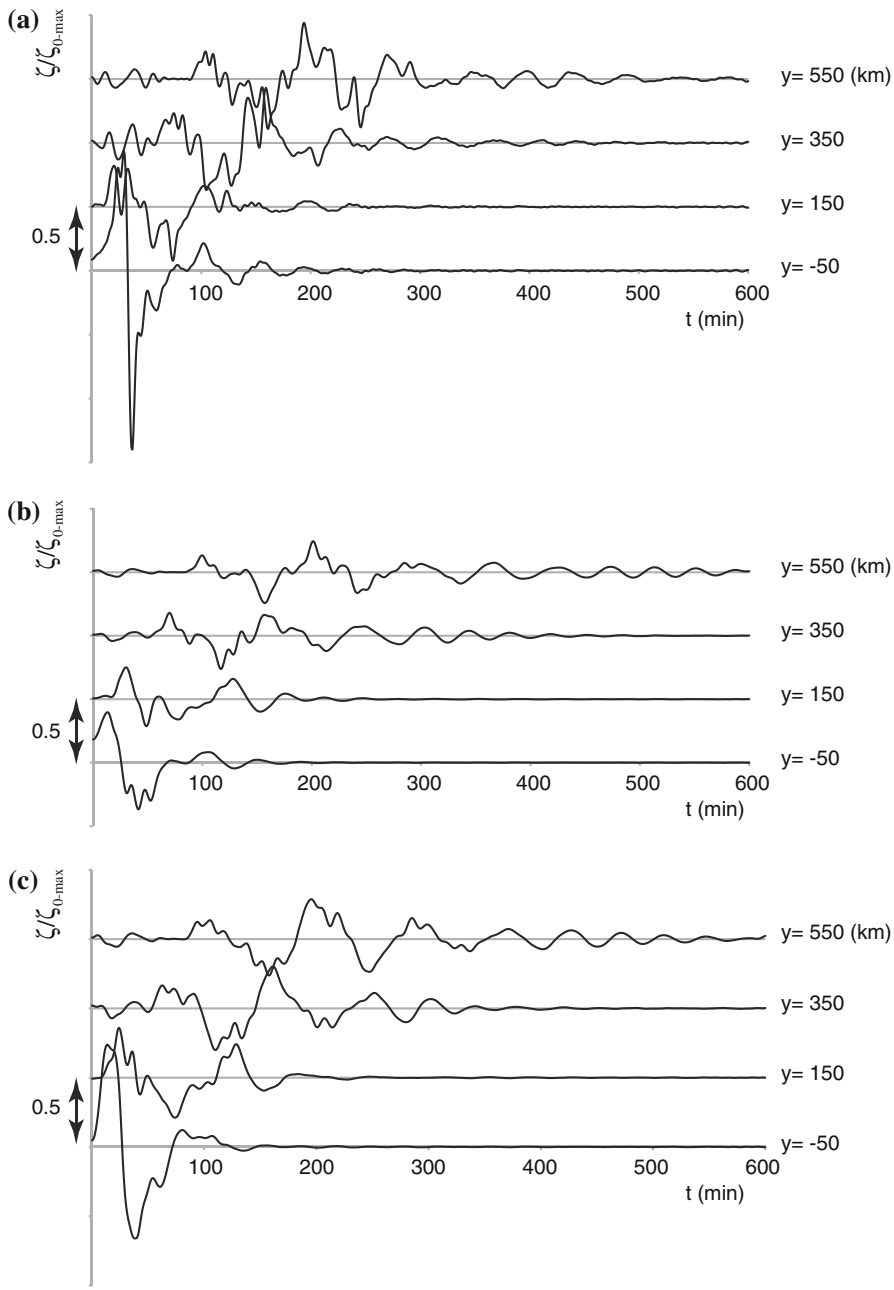

Figure 9
Time series near the coast at different longshore positions for the six slip realizations shown in Fig. 6

initial conditions were specified by earthquake mechanics and elastic deformation theory.

For the simple crack representation, I show that edge wave excitation depends on how close the vertical displacement field is to the shoreline, consistent with previous studies that use analytic representations of the initial tsunami wavefield (Fujima *et al.*, 2000; Kajiura, 1972). For crack models, the longshore variation of maximum edge wave amplitude retains a consistent pattern for each of the offshore source positions tested, whereas the more realistic stochastic slip models results in considerable longshore

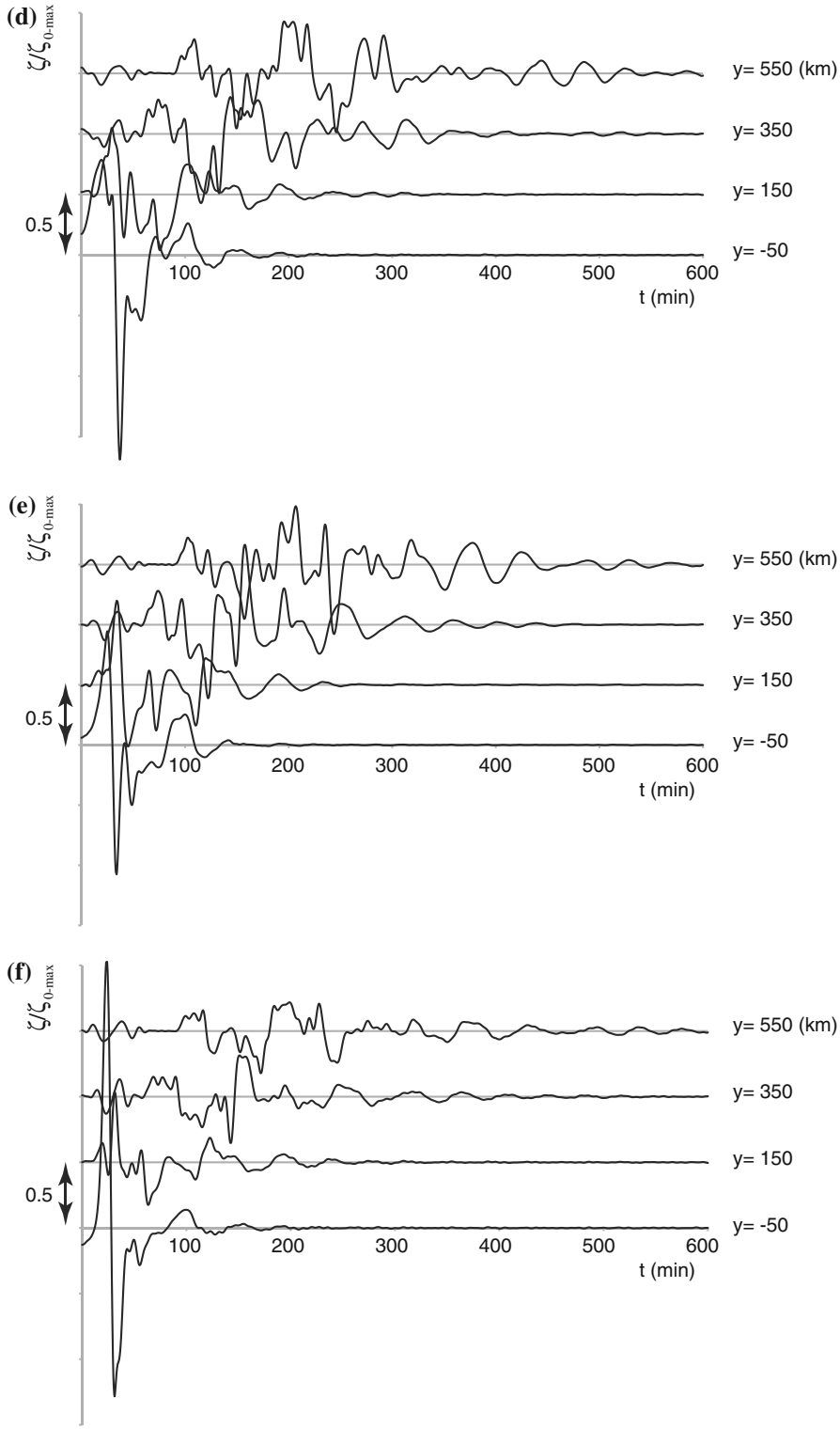

Figure 9
continued

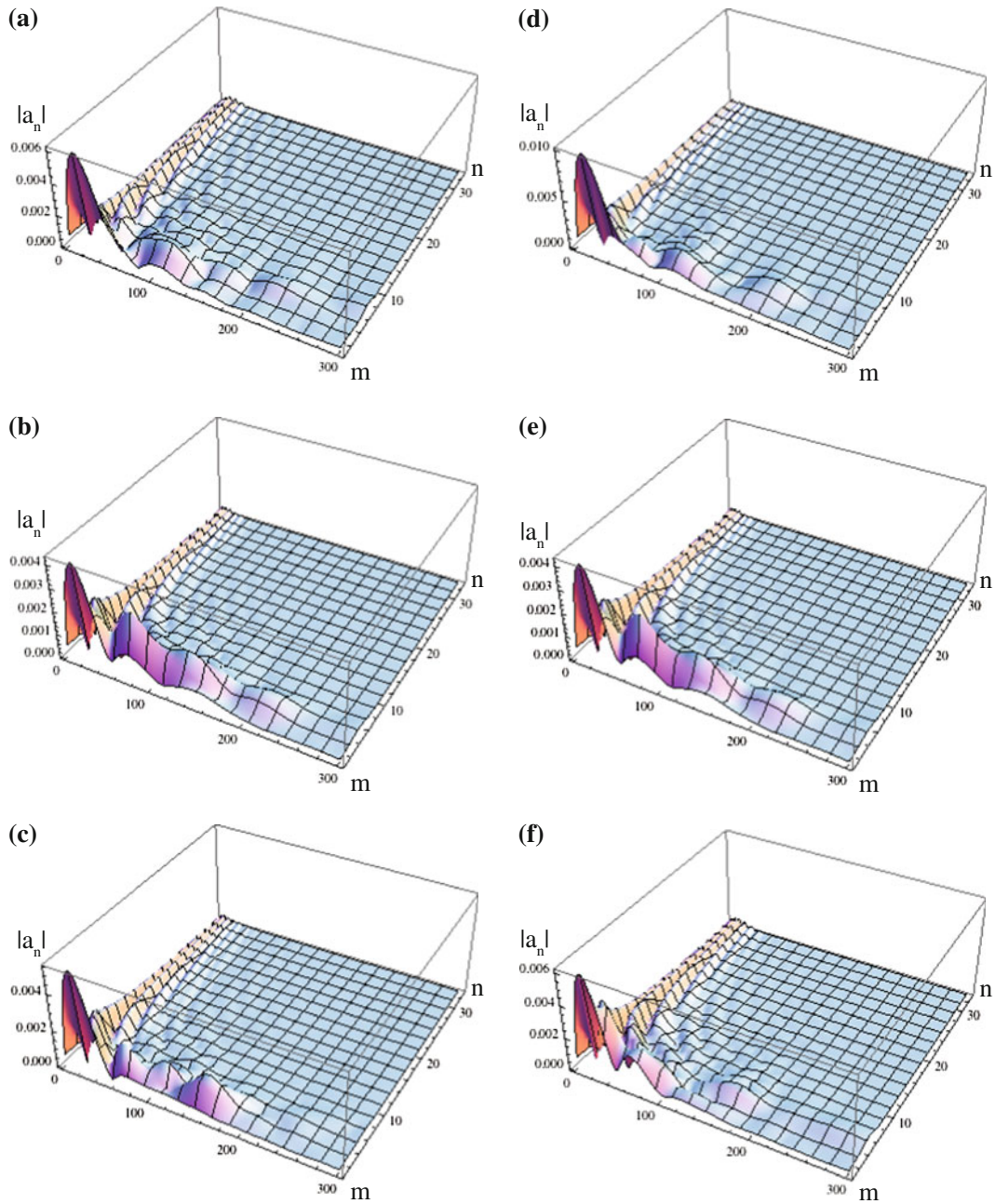

Figure 10
Series expansion coefficients (a_n) as a function of longshore Fourier spectrum (m, where $k_y = 2\pi m/(N_y \Delta_y)$) and edge-wave mode number (n) for the six slip realizations shown in Fig. 6

variability in maximum edge-wave amplitude. The model experiments presented in this study use a simple sloping bathymetry with no variation in the coastline. Introducing realistic bathymetry, coastline, and bottom friction will result in greater attenuation of edge wave energy.

Variations in the coastline can also set up interesting edge-wave effects, including resonance and

interaction of counter-propagating edge wave phases. Yamazaki and Cheung (2011) demonstrate that initially progressive edge waves can resonate in embayments and heighten tsunami amplitudes compared to non-resonant modes, as shown for the 2010 Chile continental subduction zone earthquake.

In the case where there are widely spaced irregularities such as headlands along the coast, it is also possible to have reflected or scattered edge-wave modes that are counter-propagating. In such a case, there potentially can be non-linear interaction between a triad of edge-wave modes (Hasselmann, 1966; Kenyon, 1970; Pierce and Knobloch, 1994). The triad satisfies both resonance conditions and the dispersion relation (LeBlond and Mysak, 1978). Kirby *et al.* (1998) demonstrates that two fundamental mode, counter-propagating waves can effectively transfer energy from one of the waves to the next higher mode, owing to the resonant interactions. Whether this interaction occurs for observed tsunami edge waves remains to be determined (see Kurkin and Pelinovsky, 2002).

6. Conclusions

In this study, it has been shown that rupture complexity associated with continental subduction zone earthquakes imparts a significant effect in the near field on longshore patterns of maximum edge-wave amplitude. Results from the crack models confirm that nearshore rupture and ruptures that span the shoreline are most efficient at exciting edge waves (Fujima *et al.*, 2000; Kajiura, 1972). Introduction of earthquake stress-drop heterogeneity through the use of stochastic slip models results in significant variability in the longshore distribution of maximum edge-wave amplitude. The stochastic models are constrained by seismic observations: namely, the seismic source spectrum and slip distributions determined from seismic waveform inversions. In some realizations, regions of high slip along the fault plane will be spatially distinct from each other. The static elastic Green's functions smooth the heterogeneity of slip (compare Figs. 6, 7), although in some cases there will be vertical displacement patterns that can be characterized as consisting of distinct sub-events (e.g., Fig. 7d, e). These sub-events can cause constructive interference of non-trapped modes as described by Geist and Dmowska (1999). In this study, it is also shown that the sub-events can cause constructive interference of edge-wave modes. Non-linear resonance is not modeled in the study and could be a compounding factor for counter-propagating edge waves. Results from this study emphasize that the hazard from tsunami edge-waves may be underestimated by using simple earthquake source characterizations.

Acknowledgments

The author gratefully acknowledges the constructive comments of Tom Parsons and two anonymous reviewers, as well as discussions with Bob Morton and Guy Gelfenbaum regarding field observations of the 2010 Chile tsunami.

References

Abe, K., and H. Ishii (1987), *Distribution of maximum water levels due to the Japan Sea tsunami on 26 May 1983*, Journal of the Oceanographical Society of Japan, *43*, 169-182.

Andrews, D. J. (1980), *A stochastic fault model 1. Static case*, J. Geophys. Res., *85*, 3867-3877.

Andrews, D. J., and M. Barall (2011), *Specifying initial stress for dynamic heterogeneous earthquake source models*, Bull. Seismol. Soc. Am., *101*, 2408-2417.

Bürgmann, R., M. G. Kogan, G. M. Steblov, G. Hilley, V. E. Levin, and E. Apel (2005), *Interseismic coupling and asperity distribution along the Kamchatka subduction zone*, J. Geophys. Res., *110*, doi:10.1029/2005JB003648.

Carrier, G. F. (1995), On-shelf tsunami generation and coastal propagation, in *Tsunami: Progress in Prediction, Disaster Prevention and Warning*, edited by Y. Tsuchiya and N. Shuto, pp. 1-20, Kluwer, Dordrecht, The Netherlands.

Dingemans, M. W. (1997), *Water Wave Propagation Over Uneven Bottoms: Part 1 - Linear Wave Propagation*, 471 pp., World Scientific, Singapore.

Dmowska, R., and B. V. Kostrov (1973), *A shearing crack in a semi-space under plane strain conditions*, Archives of Mechanics, *25*, 421-440.

Dmowska, R., and J. R. Rice (1986), Fracture theory and its seismological applications, in *Continuum Theories in Solid Earth Physics*, edited by R. Teisseyre, pp. 187-255, PWN-Polish Scientific Publishers, Warsaw.

Fritz, H. M., et al. (2011), *Field survey of the 27 February 2010 Chile tsunami*, Pure Appl. Geophys. *168*, 1989–2010

Fujima, K., R. Dozono, and T. Shigemura (2000), *Generation and propagation of tsunami accompanying edge waves on a uniform shelf*, Coastal Engineering Journal, *42*, 211-236.

Geist, E. L. (2002), *Complex earthquake rupture and local tsunamis*, J. Geophys. Res., *107*, doi:10.1029/2000JB000139.

Geist, E. L. (2009), *Phenomenology of tsunamis: Statistical properties from generation to runup*, Adv. Geophys., *51*, 107-169.

Geist, E. L., and R. Dmowska (1999), *Local tsunamis and distributed slip at the source*, Pure Appl. Geophys., *154*, 485-512.

Golovachev, E. V., I. E. Kochergin, and E. N. Pelinovsky (1992), *The effect of the Airy phase during propagation of edge waves*, Soviet Journal of Physical Oceanography, *3*, 1-7.

Hartzell, S. H., and T. H. Heaton (1985), *Teleseismic time functions for large, shallow, subduction zone earthquakes*, Bull. Seismol. Soc. Am., *75*, 965-1004.

Hasselmann, K. (1966), *Feynamn diagrams and interaction rules of wave–wave scattering processes*, Reviews of Geophysics, *4*, 1-32.

Herrero, A., and P. Bernard (1994), *A kinematic self-similar rupture process for earthquakes*, Bull. Seismol. Soc. Am., *84*, 1216-1228.

Ishii, H., and K. Abe (1980), *Propagation of tsunami on a linear slope between two flat regions. Part I edge wave*, Journal of Physics of the Earth, *28*, 531-541.

Johnson, J. M., and K. Satake (1999), *Asperity distribution of the 1952 Great Kamchatka earthquake and its relation to future earthquake potential in Kamchatka*, Pure Appl. Geophys., *154*, 541-553.

Kajiura, K. (1972), *The directivity of energy radiation of the tsunami generated in the vicinity of a continental shelf*, Journal of the Oceanographical Society of Japan, *28*, 260-277.

Kenyon, K. E. (1970), *A note on conservative edge wave interactions*, Deep-Sea Research, *17*, 197-201.

Kirby, J. T., U. Putrevu, and H. T. Özkan-Haller (1998), Evolution equations for edge waves and shear waves on longshore uniform beaches, in *Proceedings of 26th International Conference on Coastal Engineering*, edited, pp. 203-216, ASCE, Copenhagen, Denmark.

Kiser, E., and M. Ishii (2011), *The 2010 Mw 8.8 Chile earthquake: Triggering on multiple segments and frequency-dependent rupture behavior*, Geophys. Res. Lett., *38*, doi:10.1029/2011GL047140.

Koshimura, S., F. Imamura, and N. Shuto (1999), *Propagation of obliquely incident tsunamis on a slope Part I: Amplification of tsunamis on a continental slope*, Coastal Engineering Journal, *41*, 151-164.

Koyama, J. (1994), *General description of the complex faulting process and some empirical relations in seismology*, Journal of Physics of the Earth, *42*, 103-148.

Kurkin, A., and E. Pelinovsky (2002), *Focusing of edge waves above a sloping beach*, European Journal of Mechanics B/Fluids, *21*, 561-577.

Lavallée, D., and R. J. Archuleta (2003), *Stochastic modeling of slip spatial complexities for the 1979 Imperial Valley, California, earthquake*, Geophys. Res. Lett., *30*, doi:10.1029/2002GL015839.

Lavallée, D., P. Liu, and R. J. Archuleta (2006), *Stochastic model of heterogeneity in earthquake slip spatial distributions*, Geophys. J. Int., *165*, 622-640.

Lay, T., C. J. Ammon, H. Kanamori, K. D. Koper, O. Sufri, and A. R. Hutko (2010), *Teleseismic inversion for rupture process of the 27 February 2010 Chile (Mw 8.8) earthquake*, Geophys. Res. Lett., *37*, doi:10.1029/2010GL043379.

LeBlond, P. H., and L. A. Mysak (1978), *Waves in the Ocean*, 602 pp., Elsevier, Amseterdam.

Liu, P. L. F., H. Yeh, P. Lin, K. T. Chang, and Y. S. Cho (1998), *Generation and evolution of edge-wave packets*, Physics of Fluids, *10*, 1635-1657.

Luttrell, K. M., X. Tong, D. T. Sandwell, B. A. Brooks, and M. G. Bevis (2011), *Estimates of stress drop and crustal tectonic stress from the 27 February 2010 Maule, Chile, earthquake: Implications for fault strength*, J. Geophys. Res., *116*, doi:10.1029/2011JB008509.

Lynett, P. J., and P. L.-F. Liu (2005), *A numerical study of run-up generated by three-dimensional landslides*, J. Geophys. Res., *10*, doi:10.1029/2004JC002443.

MacInnes, B. T., R. Weiss, J. Bourgeois, and T. K. Pinegina (2010), *Slip distribution of the 1952 Kamchatka great earthquake based on near-field tsunami deposits and historical records*, Bull. Seismol. Soc. Am., *100*, 1695-1709.

Mai, P. M., and G. C. Beroza (2000), *Source scaling properties from finite-fault-rupture models*, Bull. Seismol. Soc. Am., *90*, 604-615.

Mai, P. M., and G. C. Beroza (2002), *A spatial random field model to characterize complexity in earthquake slip*, J. Geophys. Res., *107*, doi:10.1029/2001JB000588.

McCloskey, J., A. Antonioli, A. Piatanesi, K. Sieh, S. Steacy, S. S. Nalbant, M. Cocco, C. Giunchi, J. D. Huang, and P. Dunlop (2007), *Near-field propagation of tsunamis from megathrust earthquakes*, Geophys. Res. Lett., *34*, doi:10.1029/2007GL030494.

McCloskey, J., A. Antonioli, A. Piatanesi, K. Sieh, S. Steacy, S. Nalbant, M. Cocco, C. Giunchi, J. Huang, and P. Dunlop (2008), *Tsunami threat in the Indian Ocean from a future megathrust earthquake west of Sumatra*, Earth Planet. Sci. Lett., *265*, 61-81.

Mei, C. C., M. Stiassnie, and D. K.-P. Yue (2005), *Theory and applications of ocean surface waves. Part 1: Linear aspects*, 513 pp., World Scientific, Singpore.

Momoi, T. (1964), *Tsunami in the vicinity of a wave origin [I]*, Bulletin of the Earthquake Research Institute, *42*, 133-146.

Morse, P. M., and H. Feshbach (1953), *Methods of Theoretical Physics, Part I*, 997 pp., McGraw-Hill, New York.

Morton, R. A., G. Gelfenbaum, M. L. Buckley, and B. M. Richmond (2011), *Geological effects and implications of the 2010 tsunami along the central coast of Chile*, Sedimentary Geology, *242*, 34-51.

Okada, Y. (1985), *Surface deformation due to shear and tensile faults in a half-space*, Bull. Seismol. Soc. Am., *75*, 1135-1154.

Pierce, R. D., and E. Knobloch (1994), *Evolution equations for counterpropagating edge waves*, Journal of Fluid Mechanics, *264*, 137-163.

Polet, J., and H. Kanamori (2000), *Shallow subduction zone earthquakes and their tsunamigenic potential*, Geophys. J. Int., *142*, 684-702.

Pollitz, F. F., et al. (2011), *Coseismic slip distribution of the February 27, 2010 Mw 8.8 Maule, Chile earthquake*, Geophys. Res. Lett., *38*, doi:10.1029/2011GL047065.

Rabinovich, A. B., L. I. Lobkovsky, I. V. Fine, R. E. Thomson, T. N. Ivelskaya, and E. A. Kulikov (2008), *Near-source observations and modeling of the Kuril Islands tsunamis of 15 November 2006 and 13 January 2007*, Advances in Geosciences, *14*, 105-116.

Rice, J. R. (1980), The mechanics of earthquake rupture, in *Physics of the Earth's Interior*, edited by A. M. Dziewonski and E. Boschi, pp. 555-649, North Holland Publishing Company.

Rudnicki, J. W., and M. Wu (1995), *Mechanics of dip-slip faulting in an elastic half-space*, J. Geophys. Res., *100*, 22,173-22186.

Samorodnitsky, G., and M. S. Taqqu (1994), *Stable Non-Gaussian Random Processes: Stochastic Models with Infinite Variance*, 632 pp., Chapman & Hall/CRC Press, Boca Raton, Florida.

Tadepalli, S., and C. E. Synolakis (1996), *Model for the leading waves of tsunamis*, Physical Review Letters, *77*, 2141-2144.

Tanioka, Y., and K. Satake (1996), *Tsunami generation by horizontal displacement of ocean bottom*, Geophys. Res. Lett., *23*, 861-865.

Tsai, C. P. (1997), *Slip, stress drop and ground motion of earthquakes: A view from the perspective of fractional Brownian motion*, Pure Appl. Geophys., *149*, 689-706.

Ursell, F. (1952), *Edge waves on a sloping beach*, Proc. R. Soc. Lond. A, *214*, 79-97.

Wu, T. Y. (1981), *Long waves in ocean and coastal waters*, Journal of the Engineering Mechanics Division, ASCE, *107*, 501-522.

Yamazaki, Y., and K. F. Cheung (2011), *Shelf resonance and impact of near-field tsunami generated by the 2010 Chile earthquake*, Geophys. Res. Lett., *38*, doi:10.1029/2011GL047508.

(Received November 30, 2011, revised February 27, 2012, accepted April 6, 2012)